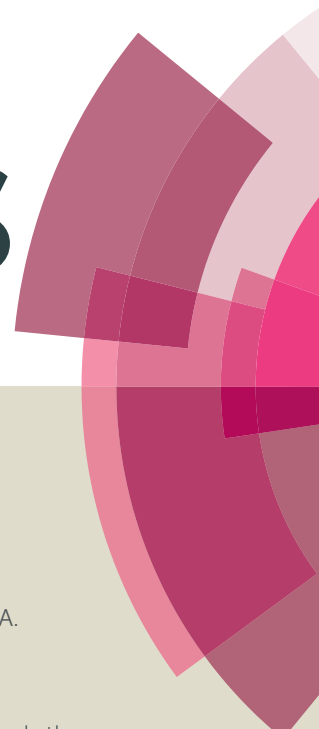


RSC Advances



This article can be cited before page numbers have been issued, to do this please use: M. Marimuthu, A. K. Venugopal, A. S. Nagpure, C. Satyanarayana and R. Thirumalaiswamy, *RSC Adv.*, 2015, DOI: 10.1039/C5RA24742J.



This is an *Accepted Manuscript*, which has been through the Royal Society of Chemistry peer review process and has been accepted for publication.

Accepted Manuscripts are published online shortly after acceptance, before technical editing, formatting and proof reading. Using this free service, authors can make their results available to the community, in citable form, before we publish the edited article. This *Accepted Manuscript* will be replaced by the edited, formatted and paginated article as soon as this is available.

You can find more information about *Accepted Manuscripts* in the [Information for Authors](#).

Please note that technical editing may introduce minor changes to the text and/or graphics, which may alter content. The journal's standard [Terms & Conditions](#) and the [Ethical guidelines](#) still apply. In no event shall the Royal Society of Chemistry be held responsible for any errors or omissions in this *Accepted Manuscript* or any consequences arising from the use of any information it contains.



Journal Name

ARTICLE

Promotional effect of Fe on performance of supported Cu catalyst for ambient pressure hydrogenation of furfural

Marimuthu Manikandan, Ashok Kumar Venugopal, Atul S. Nagpure, Satyanarayana Chilukuri* and Thirumalaiswamy Raja*

Received 00th January 20xx,
Accepted 00th January 20xx

DOI: 10.1039/x0xx00000x

www.rsc.org/

Noble-metal free FeCu based bimetallic catalyst system prepared by facile co-impregnation method was found to be a highly admirable for vapour phase selective hydrogenation of furfural to furfuryl alcohol at ambient pressure. Monometallic Cu/ γ -Al₂O₃, Fe/ γ -Al₂O₃ and bimetallic FeCu/ γ -Al₂O₃ catalysts with different Fe loadings were prepared. Structural and morphological features of the catalysts were thoroughly investigated by several physico-chemical characterization techniques. The influence of various reaction parameters, such as Fe loading, reaction temperature and flow of reactants was examined with respect to furfural conversion and furfuryl alcohol yield. The results clearly showed that the optimum amount of Fe is necessary to enhance the catalytic activity of monometallic Cu/ γ -Al₂O₃ for the selective hydrogenation of furfural. The catalyst FC-10 with a 10 wt% of Fe exhibited an excellent activity which led to high furfural conversion (>93%) and furfuryl alcohol selectivity (>98%) under mild reaction conditions. The higher activity of bimetallic Fe-Cu/ γ -Al₂O₃ compared to monometallic Cu/ γ -Al₂O₃ is ascribed by the formation of FeCu bimetallic particles and the existence of oxygen vacancies in Fe oxide system. The superior activity after Fe loading on the Cu-based catalyst was attributed to the synergy between Cu and Fe. A plausible mechanism is proposed to explain the promoting effect of Fe, which involves the synergism between Fe sites with strong oxophilic nature and Cu sites with the high ability for hydrogen activation. Based on the activity results, prolonged catalytic activity and spent catalyst analysis, the developed CuFe catalyst is inexpensive, eco-benign and robust, which makes it a promising candidate for the efficient conversion of biomass-derived substrates to fine chemicals and drop-in fossil fuels.

Introduction

Climate change, population growth and depletion of fossil fuel suggest that renewable resources will need to play a bigger role in the near future. The fundamental understanding and the efficient utilization of renewable biomass resources has become more and more attractive research area in industry and academia.¹ Lignocellulosic biomass, an unique renewable and alternative resource, can be converted into platform chemicals, value added products and fuels.¹⁻³ The selective conversion of biomass derived substrates to fine chemicals and fuels has been examined extensively over the past few decades and many studies have been shown that lignocellulosic biomass offers a great potential to be used as a sustainable feedstock.^{4,5} The immense attention has been received to develop the process for the efficient conversion of biomass to liquids, solids, gases and fuels.⁶

Furfural (FAL) is an important platform molecule, which is obtained from the dehydration of xylose, a monosaccharide often available in huge quantities in the hemicellulose fraction

of lignocellulosic biomass. In recent years, FAL has been received renewed attention as a potential platform molecule for the production of biomass-derived chemicals and drop-in biofuels.⁷ FAL can be transformed into a series of liquid fuels, fuel additives and other chemicals like furfuryl alcohol (FOL), 2-methylfuran (2-MF), methyltetrahydrofuran (MTHF), furoic acid, furan and levulinic acid, etc (Scheme 1).⁸ FOL, an essential intermediate finds many applications as solvent, ingredient in the manufacture of various chemical products such as resins, rubbers, adhesives, synthetic fibres and wetting agents, impregnating solutions, carbon binders, lubricant, dispersing agent and plastisizer.⁷ It is also used as an inert diluent for epoxy resins, resins for corrosion-resistant mortars and furan polymer concrete, modifier for urea and phenolic resins.^{8,9} Importantly, FOL is used in the production of useful organic solvents like tetrahydrofurfuryl alcohol (THFA), tetrahydrofuran (THF) and others.⁷⁻⁹ In industry, the crucial molecule FOL is generally produced by the catalytic reduction of FAL and industries adopt vapour phase hydrogenation most often due to obviate the high-priced operating costs of using batch reactors and mandatory of exorbitant apparatus for generating high pressure in the liquid phase process. Recently, efforts have

Catalysis & Inorganic Chemistry Division, CSIR-National Chemical Laboratory, Dr. Homi Bhabha Road, Pune - 411 008, India. Fax: (+) 91-20-25902633; Tel: (+) 91-20-25902006; E-mail: t.raja@ncl.res.in

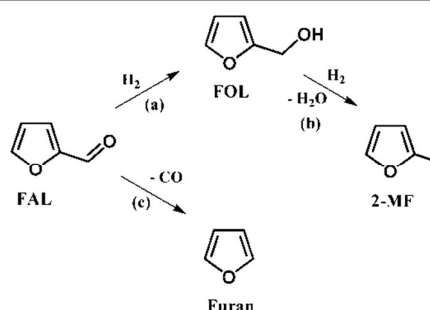
been made to carry out the conversion of FAL to FOL in vapour-phase continuous processes. Cr₂O₃-promoted Cu-based system is the conventional catalyst for the production of FOL with moderate activity and selectivity at stringent reaction conditions.¹⁰ Due to its toxicity, it causes serious environmental issues. Indeed, the evolution of innocuous Cr-free green catalysts is crucial for the efficient production of FOL.

Over the past few decades, a large number of reports are available in the literature with Cr-free catalysts for selective hydrogenation of FAL to FOL. Generally, most catalysts can hydrogenate both C=C and C=O bonds, but the control of the selective hydrogenation activity over C=C/C=O hydrogenation has one of the most important tasks for the design of an efficient hydrogenation catalyst. Cu-based catalysts are the most utilized and deliberated in industry as well as in literatures, due to its preferential C=O bond hydrogenation ability in carbonyl compounds.¹¹ B. M. Nagaraja et al. reported an excellent activity of Cu/MgO and Cu-MgO-Cr₂O₃ catalysts in FAL hydrogenation.¹² K. Yan et al. achieved 95% yield of FOL over Cu-Cr catalyst at a high reaction temperature (120–220 °C) and high hydrogen pressure (35–70 bar).¹³ Although, these catalysts showed superior performance, still it is far from satisfactory due to the toxicity and deactivation within a short period of time. Meanwhile, several heterogeneous catalysts, including both noble and non-noble metal catalysts have been reported for vapour phase as well as liquid phase hydrogenation of FAL to FOL.^{13–16} Merlo et al. reported bimetallic PtSn catalysts for the liquid phase selective hydrogenation of FAL to FOL with selectivity of 96–98% at high pressure.¹⁷ Kijenski et al. reported the use of Pt deposited on monolayer supports for hydrogenation of FAL to FOL with 93.8% of yield. Recently, more number of results are reported with noble metal catalysts.^{15–18} Regrettably, the industrial scale process of these reported catalysts is away from reality due to their cost and abundance towards commercialization. In view of the innovative aspect of the heterogeneous bimetallic catalysts, especially those based on non-precious and eco-benign, are highly demanded for various chemical processes such as hydrogenation, dehydrogenation, catalytic reforming and so on.¹⁹

Bimetallic catalysts often show electronic and chemical behavior, which are significantly distinct from their corresponding monometallic catalysts that offer the greater opportunity to tailor a novel catalyst with enhanced catalytic performance. Incorporating a second metal could be markedly altered the activity of the first one due to electronic, chemical and geometric effects.²⁰ The perceiving of these surpassing properties of bimetallic catalysts has inspired many extensive investigations on using these in catalysis. Indeed, the designing of effective supported inexpensive, non-noble metal catalysts with outstanding activity is a strenuous task for researchers.²¹ The applications of first row transition metals in a variety of chemical transformations are well-known phenomenon. For example, Cu serves an exceptional behavior, which is competing for noble metals based catalysts in salient research fields.²² In this work, we have chosen Cu as an active component based on the reported literatures and aimed to

minimize the undesired products by adding another metal in order to enhance its activity, stability and selectivity.^{8,14} As mentioned earlier, it is possible to tune the reactivity and selectivity of Cu by the addition of another element like Fe. Because Fe has redox behavior like cerium and zirconium, which are usually accounted for the efficient performance by providing the synergistic interaction. In addition, Fe has a higher oxygen affinity and oxygen vacancies which can facilitate the reaction by binding and subsequently activating the oxygenates.²³ Recently, Sithisa et al. showed superior activity of FeNi/SiO₂ catalysts in the conversion of FAL to 2-MF.²⁴ Also, the incorporation of inexpensive Fe on Cu-based heterogeneous catalysts for various catalytic transformations have been studied in many reports.^{23–25} Addition of Fe could inhibit the sintering of Cu and also enhances the active surface area of Cu. Moreover, it can also promote the catalytic activity due to the synergistic interaction between Cu and Fe.^{26,27} However, the systematic investigation of CuFe catalyst system for hydrogenation of FAL to FOL is rarely disclosed.

Herein, we present the work aiming toward the efficient development of high-performance catalyst for the selective hydrogenation of FAL to FOL at ambient pressure. The efforts have been made to prepare γ -Al₂O₃ supported Cu, Fe and FeCu catalysts with different Fe wt% and investigated the effect of Fe on the catalyst performance in the selective hydrogenation of FAL. The excellent yield (~92%) of FOL was obtained over FC-10 catalyst under optimized reaction conditions, which is much higher than that of the commercial catalyst (Cu-1800P), which gave FAL conversion of 65% with 99% selectivity towards FOL.¹² We found that the product distribution was highly influenced by the Fe loading, reaction temperature and contact time of the reactant. Moreover, the effect of various reaction parameters and catalytic stability were also studied. Mainly, the results are contributing to understanding the origin of the promotional effect of Fe and the design of greatly admirable catalyst for selective hydrogenation of FAL to FOL. The results reported in the present investigation may inspire to start focusing on the inexpensive non-noble metal based catalysts for the selective conversion of biomass derived furanic compounds to value added chemicals and fuels.



Scheme 1. Reaction routes for the hydrogenation of FAL to FOL and other possible products. (a) Hydrogenation, (b) hydrogenolysis, and (c) decarbonylation.

Results and Discussion

Characterizations of pre-catalysts

Structural characteristics of the pre-catalysts were examined by powder XRD analysis. Fig. 1 shows the XRD patterns of the pre-catalysts. All diffraction features were indexed with both γ - Al_2O_3 and Fe_2O_3 . γ - Al_2O_3 exhibits strong diffraction peaks at $2\theta=33^\circ$, 37.4° , 46° and 66.7° .²⁸ For F-10 pre-catalyst, the weak reflections at 33.34° , 35.66° , 49.8° and 54.4° are ascribed to Fe_2O_3 (JCPDS # 65-7002).²⁷ The diffraction peaks related to FeO and Fe_3O_4 were not observed in XRD. No apparent peaks attributable to CuO were observed for the C-10 and other Cu containing pre-catalysts suggesting that Cu is present as amorphous or in highly dispersed form. Likewise, the patterns for pre-catalysts from FC-2.5 to FC-10, absence of the corresponding peaks for both Fe_2O_3 and CuO demonstrated that both species are also present as highly dispersed nanocrystalline, or amorphous form.²⁸ Moreover, the pre-catalyst with maximum Fe loading (FC-12.5) shows the reflections for corresponding Fe_2O_3 features, which evidences the formation of large crystallites after certain loading. According to the obtained results, it is found that there was an interaction between iron and copper oxides, promoting the dispersion of both species. This is further substantiated by H_2 -TPR results

H_2 -TPR profiles of all calcined catalysts are depicted in Fig. 2. H_2 -TPR profile for C-10 pre-catalyst exhibited a symmetrical reduction peak at about 181.4°C which could be attributed to the reduction of CuO species. Literature reports suggested that the supported Cu catalysts show two H_2 consumption peaks, which are assigned to the reduction of well dispersed and Cu^{2+} species having a strong interaction with the matrix.^{29,30} The observed result for C-10 pre-catalyst is much lower than the reported values which might be due to the presence of isolated highly-dispersed CuO species. For F-10 pre-catalyst, H_2 -TPR is distinctively different from those of others. The first peak located maximum at 396°C is attributed to the reduction of Fe_2O_3 to Fe_3O_4 and the second peak (not shown here) above

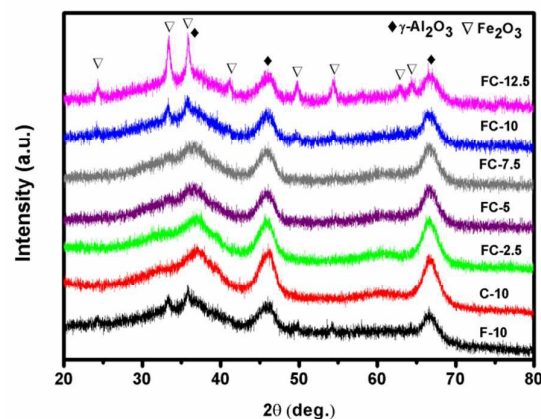


Fig.1 XRD patterns of the γ - Al_2O_3 supported Fe, Cu, and FC-X pre-catalysts.

800°C is associated with the reduction of magnetite to metallic Fe.^{26,31} In contrast to the F-10 pre-catalyst, bimetallic FC-X pre-catalysts did not display any peaks above 400°C . This inference is evidence that the simultaneous reduction of iron oxide species with copper oxides. Clearly, Cu promoted the reducibility of iron oxides, consistent with other investigations.³¹ This is further established by the increasing H_2 consumption with the increasing Fe loading in the bimetallic samples (Table 1), since Cu loading is kept constant and complete reduction of F-10 sample is much difficult below 500°C . The promotion effect might be due to facile H_2 dissociation on Cu followed by spillover of hydrogen to magnetite phase.³¹ Furthermore, as the Fe content increases, the high-temperature peak shift to a low temperature region, evidenced the weakened interaction between Cu and the support, which is also indicating the strong interaction between Fe and Cu. This could be also attributed to the synergistic electronic interaction between Fe and Cu. For FC-12.5 pre-catalyst, a slight peak shift towards higher temperature along with a new peak around 300°C suggested that in higher Fe loading causes large crystallites after a certain

Table 1. Physico-chemical properties of the γ - Al_2O_3 supported metal catalysts

| Entry | Catalyst | Surface area (m^2g^{-1}) ^[a] | Average pore size ^[b] (nm) | Total pore volume ^[b] (cc/g) | Cu particle Size ^[c] (nm) | Cu metal dispersion ^[d] (%) | Cu metal Surface area (m^2g^{-1}) ^[d] | H_2 consumption from TPR ($\text{mmol g}^{-1}\text{ cat}$) |
|-------|------------------------------------|---|---------------------------------------|---|--------------------------------------|--|--|---|
| 1 | γ - Al_2O_3 | 182.0 | 11.3 | 1.0 | --- | --- | --- | --- |
| 2 | C-10 | 202.6 | 11.0 | 0.71 | 8.4 | 26.1 | 10.8 | 13.4 |
| 3 | FC-2.5 | 216.1 | 11.1 | 0.57 | 8.1 | 32.3 | 12.0 | 13.5 |
| 4 | FC-5 | 219.7 | 11.4 | 0.59 | 7.9 | 33.5 | 13.4 | 13.9 |
| 5 | FC-7.5 | 224.6 | 10.9 | 0.61 | 7.9 | 34.9 | 13.7 | 14.2 |
| 6 | FC-10 | 205.8 | 10.8 | 0.58 | 8.2 | 36.6 | 14.6 | 14.6 |
| 7 | FC-12.5 | 151.8 | 7.6 | 0.48 | 10.3 | 30.8 | 10.2 | 14.4 |
| 8 | F-10 | 217.8 | 10.7 | 0.64 | 7.1 | --- | --- | 0.67 |
| 9 | Spent C-10 | 172.4 | 7.9 | 0.42 | 11.7 | n.d | n.d | n.d |
| 10 | Spent FC-10 | 193.8 | 9.4 | 0.46 | 9.1 | n.d | n.d | n.d |

[a] Specific surface area calculated using the BET method. [b] Calculated from BJH method. [c] Calculated from TEM analysis. [d] Determined by H_2 - N_2O titration.

limit, as evidenced by XRD results. Finally, the H₂-TPR profiles allow us to conclude that Fe and Cu species forming bimetallic system.

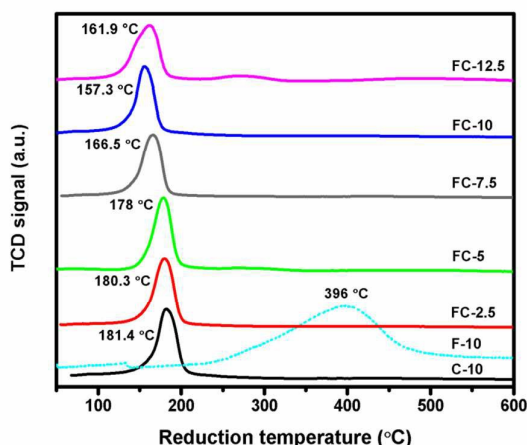


Fig. 2 TPR profiles of the γ -Al₂O₃ supported F-10 (dash line), C-10 and FC-X pre-catalysts.

The textural characteristics of γ -Al₂O₃ based catalysts were examined by N₂ adsorption-desorption, pore-size distribution analysis and the results are shown in Fig. S1 (ESI) and Table 1. All catalysts show type IV isotherm with H4 hysteresis loops (Fig. S1a) which is typical for mesoporous materials. Pore size distribution (Fig. S1b) of the catalysts shows that the pores are falling within the uniform range (8–12 nm). The BET surface area increases marginally from 182 to 202.6 m²g⁻¹ for γ -Al₂O₃ and C-10 respectively, which might be due well-dispersed Cu oxides. The BET surface area of FC-2.5 and FC-5 pre-catalysts were slightly increased with the increase of Fe content and then marginally decreased for FC-7 and FC-10. The change in particle size in the same trend is accounting for the transition in surface area of the pre-catalysts. The pre-catalyst containing highest Fe loading exhibited the decrease in surface area which might be due to the agglomeration. Compared to the C-10 sample, bimetallic samples (FC-X) showed more surface area indicated that the addition of Fe promoted the surface area of monometallic samples. XRD of the FC-10 catalysts also substantiated the high dispersion of Fe and Cu species which leads to give more surface area. Moreover, increasing surface area after the metal loadings of the promoter is a well-known phenomenon, which was explained elsewhere.^{32,33}

Characterization of catalysts

The XRD patterns of reduced catalysts are given in Fig. S2 (ESI). For all the catalysts, diffraction patterns are predominantly attributed to the reflections of γ -Al₂O₃. No discernible peaks were observed for both Fe and Cu metallic features as in the catalysts are corroborated that the highly dispersed nature of both species. For bimetallic FC-12.5 catalyst, a peak appeared at 30.3° and 35.6° was attributed to the (200) and (311) planes of Fe₃O₄ (JCPDS #75-0033), respectively.³⁴ However, a small reflection at 44.6° is the indicative of the presence of iron metallic species. In all

patterns, the absence of metallic copper or cuprous oxide signals suggested that either well dispersion or overlapped peaks with Fe₃O₄ at 35.6°. As shown in Table 1, the Cu dispersion was measured by H₂-N₂O titration, which increases monotonically from 26.1 to 36.6% with the increasing Fe loading up to 10 wt%, then it showed a marginal decrease. The observed results are highly consistent with the change in the size of the Cu particles determined by the TEM analysis. As a result, the addition of a large amount of Fe is not helpful for the higher dispersion, which is reflected as the decrease in dispersion at higher Fe loading (FC-12.5, Table 1, entry 7). Generally, a high specific surface area can result in a good metal dispersion.¹¹ In the present catalyst system, the BET specific surface area of the FeCu/ γ -Al₂O₃ samples increases gradually with the Fe loading (Table 1), which is associated mainly with the increase in the content of the Fe. Meanwhile, Cu surface areas exhibit a slight increasing trend with the Fe loading from 2.5 to 10 wt%, indicative of the increase in the surface metallic Cu sites. However, the FC-12.5 sample has the smallest Cu surface area (10.2 m² g⁻¹), which should be ascribed to the agglomeration or surface coverage of Fe species.

To study the reduction behavior of both Fe and Cu in more detail, the most active FC-10 catalyst was examined for the *in-situ* XRD analysis with different temperatures (27–400 °C) in the presence of H₂ flow (30 mL min⁻¹). As shown in Fig. 3, the diffraction patterns were recorded at 27, 200, 250, 300, 350 and 400 °C with the scanning rate of 0.4° min⁻¹, temperature was allowed to stabilize prior to each scan. XRD profile emphasized that the CuO was started reduced to Cu₂O/metallic copper at 200 °C ($2\theta=43.2$ and 50.3°), which is accordance with the literature values.³⁵ No corresponding peaks were observed for reduced Fe species at this temperature, which might be due to the insufficient temperature for reduction of Fe³⁺ to Fe⁰. The appearance of metallic phases by increasing temperature unveils that the reduction of both Fe and Cu at 400 °C. The obtained results concluded that the bimetallic FeCu species were formed upon pre-treatment at 400 °C.³⁶

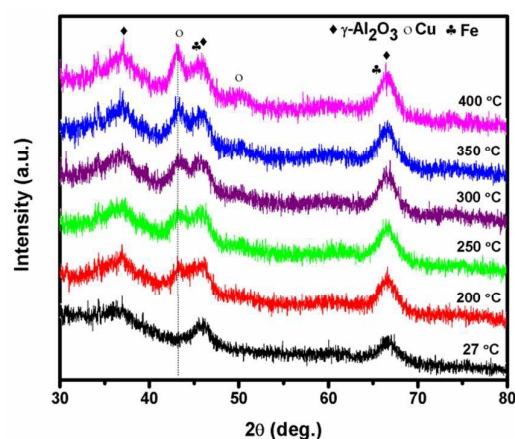


Fig. 3 XRD patterns of the FC-10 catalyst during *in-situ* reduction with different temperatures at 40 mL min⁻¹ flow of H₂.

Morphological aspects of the reduced monometallic C-10, F-10 and bimetallic FC-10 catalysts were studied by TEM analysis and the results are shown in Fig. 4. For C-10 catalyst (Fig. 4a), uniform needles like morphology with spherical particles was noticed, which is usually observed for γ -alumina supported materials.²⁸ However, the clear interface between the copper phase and the support is difficult to be identified, due to poor contrast between the metal and the support.³⁰ TEM image of F-10 (Fig. 4b) also shows good dispersion with dark particles. The calculated interlayer distances 0.251 and 0.294 nm due to the (311) and (220) phases of Fe_2O_3 , which are in good accordance with XRD results. No discrete Cu or Fe

particles were observed in both cases, which proved the amorphous or nanocrystalline behavior. This aspect can be further confirmed by the SAED patterns (Fig. 4 insets). The reduction behavior of FC-10 catalyst is distinctly differs from the monometallic catalysts. As shown in Fig. 4d-f, TEM images of FC-10 clearly exhibited that bimetallic FeCu nanoclusters (Fig. 4f) without agglomeration of particles are highly dispersed on the support. The average particle size of Cu in FC-10 catalyst is 8.2 nm (Fig. 4f). The observed interlayer distances shows dominant oxide features (Fe_3O_4 and Cu_2O) as evidenced from XRD of reduced catalysts.

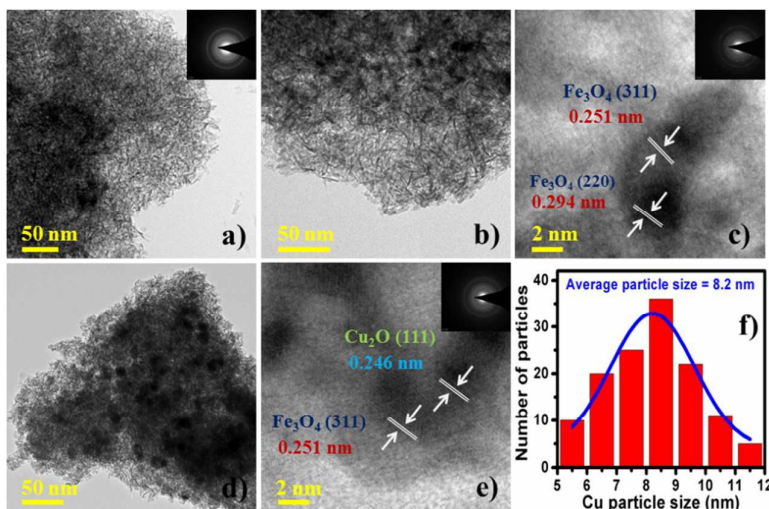


Fig. 4 TEM images of reduced samples (a) C-10, (b, c) F-10 and (d-e) FC-10. (f) Particle size distribution of the FC-10 catalyst.

To understand the more insights into the surface chemical states of Fe and Cu in the FC-10 catalyst during catalysis, the *in situ* XPS analysis was performed. The catalyst was placed inside the XPS chamber and heated to different temperatures in the presence of 0.1 mbar H_2 pressure. The core level spectrums were recorded at Ultra High Vacuum (UHV) followed by room temperature (RT), 250 and 400 °C under 0.1 mbar H_2 pressure; the temperatures were kept constant for 2 hours prior to each recording. The photoemission features of both Fe and Cu 2p core levels are shown in Fig. 5a and 5b, respectively. For the survey scan of Fe ($2p_{3/2}$) presented in Fig. 5a, the binding energy observed at 711.4 and 724.2 eV and their satellite features evidenced that the surface phase at UHV and RT is Fe_2O_3 .³⁶ No peaks were seen for reduced Fe species on treatment at 250 °C, which might be due to the insufficient reduction temperature. Upon reduction at 400 °C, the binding energy values at 707.6 and 720.8 eV corroborated that Fe_2O_3 was reduced to Fe_3O_4 and further to metallic Fe.^{36,37}

The spectra recorded at UHV and RT (Fig. 5b) shows predominant spin orbit peaks for $\text{Cu}2p_{3/2}$ and $\text{Cu}2p_{1/2}$ binding energy values at 934.8 ± 0.2 and 955 eV, respectively, which are in good accordance with the reported literature.³⁸⁻⁴⁰ Moreover, the presence of Cu^{2+} state is confirmed by the observation of satellite features around 942 eV. Upon treatment at 250 °C in 0.1 mbar H_2 , the position of $\text{Cu}2p_{3/2}$ down-shifted to 932.6 eV.

Clearly, Cu^{2+} was reduced to Cu^0 , such a binding energy value is slightly deviates apart from those reported in the literature, indicates that the chemical environment of the Cu changes, presumably owing to the interaction of Cu with Fe species during the activating process. Meanwhile, the appearance of Cu 2p satellite peaks implying the existence of both Cu^+/Cu^0 species. Furthermore, the recorded spectra at 400 °C clearly proved that the complete reduction of CuO to metallic Cu (B.E = 932.3 eV).⁴¹ Further analysis using the Auger parameter confirmed that the presence of metallic Cu (567.9 eV) instead of Cu^+ after reduction at 400 °C (Fig. S3). The observed binding energy values for Oxygen 1s core levels were also in great agreement with the above conclusions.

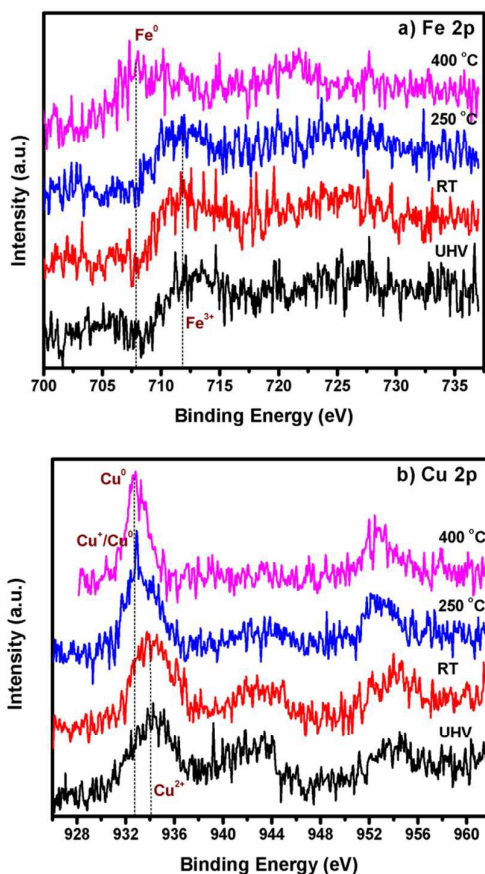


Fig. 5 *In situ* XPS spectra recorded for a) Fe 2p and b) Cu 2p core level of bimetallic FC-10 catalyst at different temperatures under UHV and 0.1 mbar H₂.

Catalytic performance

We began our studies with the effect of different metal loadings and followed to test on various reaction parameters on the conversion of FAL to FOL. Under the studied reaction conditions the main products were: FOL, 2-MF and Furan. The results are given in Table 2. The conversion of FAL was <90% of all samples except for entry 6 (93%), whereas the selectivity of FOL was >90% for all catalysts except for F-10 (entry 2 and 8). This dissimilar was extensively discussed by studying the selective hydrogenation of FAL by using various Fe content and by keeping the Cu content same. We have also investigated the influence of experimental conditions on the product distribution over bimetallic FC-10 and monometallic F-10 and C-10 catalysts for comparison. A control experiment, loading the reactor tube with γ -alumina was conducted under the optimized reaction conditions which exhibited scarce conversion of FAL.

Effect of Fe loading

Fig. 6 displays the effect of the Fe wt% loading on the catalyst activity. Fig. 6 (a) indicates that C-10 had a much higher conversion for hydrogenation of FAL than F-10. However, the

Table 2. Product distributions during FAL hydrogenation over different catalysts.^[a]

| Entry | Catalyst | FAL Conversion (mol %) | Selectivity (mol %) | | |
|-------|--|------------------------|---------------------|------|-------|
| | | | FOL | 2-MF | Furan |
| 1 | γ -Al ₂ O ₃ | 3.6 | --- | --- | Trace |
| 2 | C-10 | 62.0 | 87.8 | 5.8 | 6.4 |
| 3 | FC-2.5 | 66.2 | 90.7 | 4.5 | 4.8 |
| 4 | FC-5 | 72.1 | 91.2 | 4.1 | 4.2 |
| 5 | FC-7.5 | 81.0 | 92.3 | 3.4 | 3.3 |
| 6 | FC-10 | 93.4 | 98.6 | 1.3 | 0.6 |
| 7 | FC-12.5 | 84.6 | 91.3 | 7.4 | 0.5 |
| 8 | F-10 | 23.2 | 12.4 | --- | --- |

[a] Activity results were at steady state under the optimized reaction condition, i.e. 175 °C, LHSV = 1 h⁻¹ with respect to FAL and GHSV = 1200 h⁻¹ with respect to H₂, 1 atm. pressure and 1 mL catalyst.

addition of Fe presented a promoting effect on the activity of C-10. As the Fe content increased, the conversion exhibited a slight volcano curve and reached the maximum at the 10 wt% of Fe. In clearer, the conversion increased from 62 to 93.4% at 175 °C and from 90 to 100% at 250 °C with Fe loading increased from 0 to 10 wt%. Among all the catalysts tested, FC-10 gave an excellent conversion in all reaction temperatures. Clearly, an optimum Fe loading is needed for the enhancing the catalytic activity of the monometallic C-10 catalyst.

Fig. 6b shows the product distribution of FAL hydrogenation with varied Fe loadings. As shown in Fig. 6b, the dominant hydrogenated product on C-10 and FC-X catalyst is FOL. Furthermore, the addition of Fe to C-10 significantly changed the product distributions. As Fe loading increased, the selectivity of FOL is increased, whereas the selectivity of 2-MF and Furan were decreased. In clearer, C-10 catalyst showed 87.8, 5.8 and 6.4% selectivity to FOL, 2-MF and Furan, respectively at 175 °C. However, the selectivity of FOL decreased to 50% and selectivity of Furan increased to 29% at 250 °C. With increasing the reaction temperature the decarbonylation (C-C cleavage) of the FAL is more favourable over C-10 catalyst. For bimetallic FC-X catalysts, the selectivity to decarbonylation product is very less (<10%) at all temperatures. It is concluded that the addition of Fe to C-10 diminished the selectivity to Furan but enhanced the selectivity to FOL. Among all, catalyst FC-10 gave better selectivity to FOL at all temperatures employed. Furthermore, selectivity of FOL for all FC-X catalysts were almost above 90% at 175 °C, which implies that the selectivity mainly depends on Cu, whereas, FAL conversion depends on the cooperative interaction between Fe and Cu. The evaluated results were concluded that the introduction of Fe into the Cu-based catalyst can promote the catalytic activity and selectivity. It has allowed us to suggest that this promoting effect results from the synergistic interaction between Cu and Fe.³⁶ Furthermore, the appropriate Fe/Cu ratio helps to achieve an excellent yield of FOL over others. From the results FC-10 is optimized as the best catalyst and it is used for further studies.

As mentioned above, the selectivity to C-C the cleavage product was remarkably reduced by the addition of Fe to C-10. This is also related to the formation of FeCu bimetallic

interaction in the catalytic system. However, the formation of FeCu bimetallic synergism with Fe enriched surface leads to the interference of the C–C hydrogenolysis at higher temperatures. Besides, Cu has also been known for decreasing the C–C hydrogenolysis activity due to its strong repulsion against furan ring.⁴¹ It is found that the decarbonylation and hydrogenation are not strongly dependent on conversion but mainly depend on reaction temperature.⁴²

Effect of reaction conditions

Fig. 6 also shows the effect of reaction temperature on the performance of different catalysts. In all cases, increasing temperature promoted the conversion of FAL due to the increased reaction rate. As the temperature increased from 175 to 250 °C, the selectivity to FOL significantly decreased and selectivity to 2-MF and Furan increased consequently because high temperature favoured the hydrodeoxygenation and decarbonylation of FAL, respectively. At higher temperatures, the decreased selectivity to FOL is ascribed to the enhanced cracking reaction. It is remarkable that the effect of reaction temperature on the selectivity of cracked product is more conclusive for C-10 as compared to bimetallic FC-X catalysts. This further substantiates that the formation of FeCu bimetallic interaction is significant for the superior performance of bimetallic FC-X catalytic system.

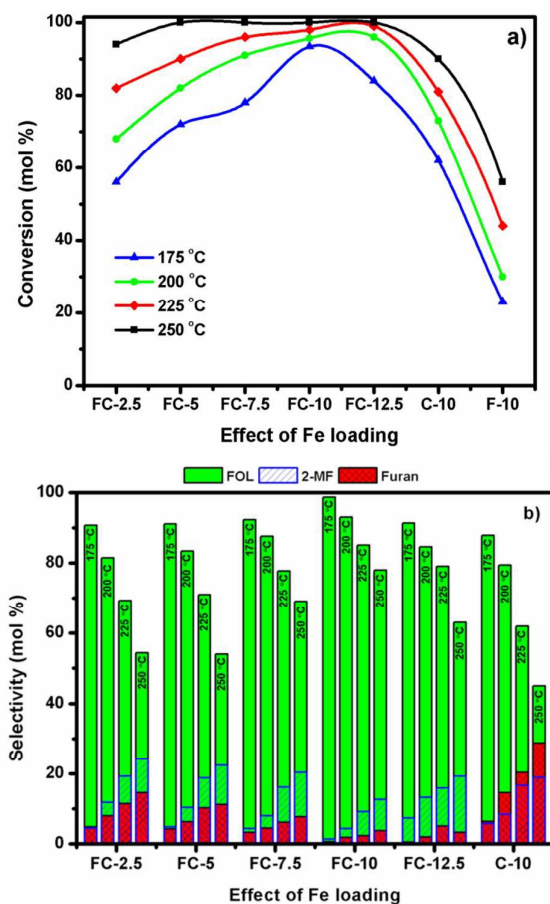


Fig. 6 Performance of selective hydrogenation of FAL as a function of reaction temperature and Fe loadings. a) FAL conversion and b) Selectivity of FOL and side products include 2-MF and Furan. Reaction conditions: LHSV=1 h⁻¹ with respect to FAL and GHSV=1200 h⁻¹ with respect to H₂, 1 atm. pressure and 1 mL catalyst. (S=Selectivity).

Since FC-10 exhibited a superior selective hydrogenation performance, the effects of LHSV (Liquid Hourly Space Velocity) and GHSV (Gas Hourly Space Velocity) on product distributions during hydrogenation of FAL were discussed. Fig. 7 shows the effect of LHSV of FAL on the performance of the FC-10 catalyst. As the LHSV of FAL rose from 1 to 2.5 h⁻¹ both the conversion and FOL selectivity decreased from 93.4 to 74.6% and from 98.6 to 82.5%, respectively, while the selectivity of 2-MF and Furan increased slightly, indicating the selective hydrogenation performance is decreased with increased LHSV. The decreased contact time with increased LHSV also account for the decrease in selectivity. Furthermore, the increased flow of FAL enhanced the coke formation might be due to the formation of polymeric species on the catalyst surface.

The effect of GHSV of hydrogen on the performance FC-10 catalyst is shown in Fig. 8. For increased GHSV from 600 to 3000 h⁻¹ the conversion and the selectivity to FOL tended to decrease slightly, while the selectivity to 2-MF increased slightly with the rise of GHSV. This seems to indicate that the increase of GHSV favours the C–O hydrogenolysis, which is plausibly due to the increased hydrogen concentration on the catalyst surface. No considerable variation in activity results at all GHSV shows thus the hydrogenation of FAL follows pseudo first order kinetics.⁴³

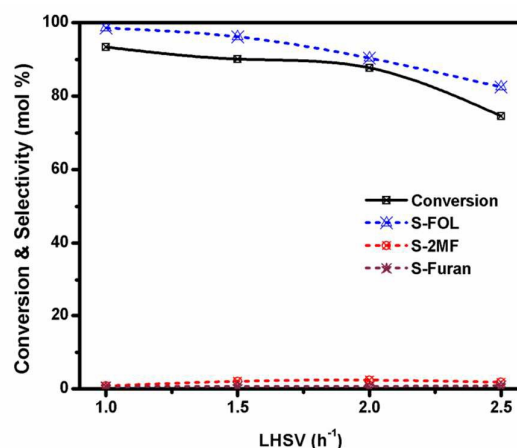


Fig. 7 Conversion of FAL and selectivity of FOL at various LHSV of FAL over bimetallic FC-10 catalyst. Reaction conditions: 175 °C, GHSV=1200 h⁻¹ with respect to H₂, 1 atm. pressure and 1 mL catalyst. (S=Selectivity)

Stability of Catalyst

To underpin the stability of the monometallic C-10 and bimetallic FC-10 catalyst, hydrogenation of FAL reaction was carried out for a longer time on stream (TOS, 24 hours) under the optimized reaction conditions. Fig. 9 shows the conversion and selectivity to FOL. As shown in Fig. 10, C-10 catalyst shows a maximum conversion (62%) and FOL selectivity (87.8%),

while both conversion and selectivity decreased with prolonging the reaction time. It is noteworthy that the C-10 has less stability, indicating the agglomeration of Cu particle after certain period. In contrast with C-10 activity, bimetallic FC-10 catalyst exhibited the steady state catalytic activity even up to 24 hours. Almost 94% conversion and >98% selectivity were achieved with a marginal decline of catalytic activity. This kind of stable activity was rarely reported due to the coke deposition during the by-product formation in the conversion of biomass derived substrates. Generally, stability of the catalyst is mainly depends on the coke deposition during reaction course, herein C-C cleavage is the strong possibility for the coke formation. It is also evidence that the addition of Fe preventing the sintering of Cu and also inhibits the Cu agglomeration on surfaces during the reaction. Besides, we concluded that the addition of Fe depleting the C-C cleavage through synergistic FeCu bimetallic interaction, which might be the reason for less or trivial by-products (<5%) and longer stability.

To perceive the properties of catalyst after TOS, both C-10 and FC-10 spent catalysts were characterized and shown in Fig. 10. We exempted XRD analysis since all catalysts exhibited high dispersion. TEM image of FC-10 spent catalyst clearly depicts that there is no morphological change even after 24 hours of reaction time, whereas the C-10 catalyst showed agglomeration. From the Cu particle sizes after reaction for 24 hours, it was found that increase in particle size for C-10 (11.7 nm) as compared to FC-10 (9.1 nm) implies that the sintering

surface area from 202.6 to 172.4 m² g⁻¹ (Table 1) for C-10 spent catalyst also accounts for this decline in activity. The ICP-OES analysis of the spent catalysts and the product mixtures shows that there is no leaching of metal. The observed results conclude that the developed catalyst system is robust and displayed an admirable catalytic activity for the selective hydrogenation of FAL to FOL and it can be applied to the hydrogenation of various biomass derived substrates to obtain value added chemicals and fuels.

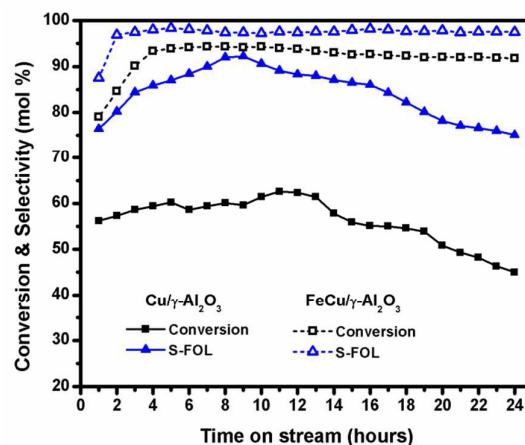


Fig. 9 Conversion of FAL and selectivity of FOL for 24 hours TOS over C-10 and FC-10 catalyst. Reaction conditions: 175°C, 1 atm. LHSV=1 h⁻¹ with respect to FAL and GHSV=1200 h⁻¹ with respect to H₂, 1 atm. pressure and 1 mL catalyst. (S=Selectivity)

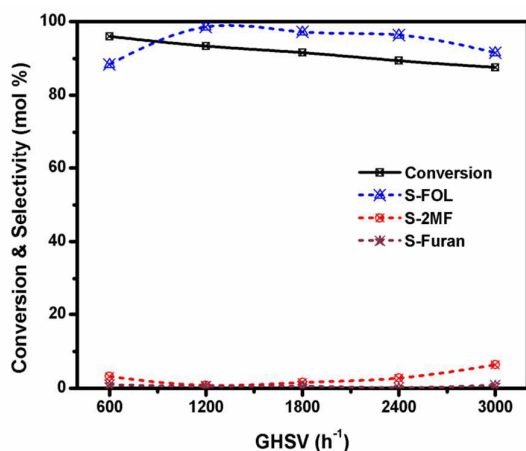


Fig. 8 Conversion of FAL and selectivity of FOL at various GHSV of hydrogen over bimetallic FC-10 catalyst. Reaction conditions: 175°C, LHSV=1 h⁻¹ with respect to FAL, 1 atm. pressure and 1 mL catalyst. (S=Selectivity)

of metal particles on C-10 was more serious than that on FC-10 (Table 1, entry 10, 11). It is evidence that the addition of Fe inhibited growth of Cu particles. The change in the morphology of the monometallic C-10 catalyst as compared with bimetallic FC-10 attributed to the decline in the activity. The recorded XPS spectrum of spent catalyst proves the presence of Cu⁰ (B.E value of 933.3 eV) and Cu²⁺ (B.E value of 935.3 eV), the availability of Cu⁰ species are the most probable active centers for the prolonged catalytic activity. Moreover, the decrease in

Plausible mechanism

The exact mechanistic pathway for the reduction of C=O group of FAL to FOL on catalytic surface is not fully understood. Although the kinetics and mechanism for FAL hydrogenation activity were discussed by Resasco *et al.* and other groups,^{41,42} the origin of the activity on bimetallic catalyst systems are still unclear. The observed results from *in situ* XRD and XPS investigations provide some new and critical information about the reducibility of both Fe and Cu. Reduction treatment provided reduced Cu as well as Fe particles and those are in close proximity. In mechanistic view, adsorption of C=O and C=C of FAL on FeCu/γ-Al₂O₃ surface are the two prospects of adsorption modes for the formation of FOL. There are considerable reports were available for the mechanism of both possibilities.^{42,46} Since metallic Cu surfaces have a very weak affinity to C=C bonds, and α,β-unsaturated aldehydes, including FAL,²⁴ implied that the adsorption of FAL on Cu results in an η¹(O)-surface species, in which the carbonyl group is bound to the metal through the oxygen lone pair while the rest of the molecule is pushed away from the surface due to a net repulsion between C=C and Cu. The preferred adsorption in the η¹(O)-mode is responsible for the high hydrogenation selectivity to FOL, typically observed on Cu-based catalysts. In our studies, no ring hydrogenated products were observed at any temperature, LHSV as well as GHSV (Fig. S4 and S5, GC-MS data, ESI), which indicates the Cu surface is strongly interacting with FAL via C=O and strongly repulsing furan ring (Scheme 2).⁴²

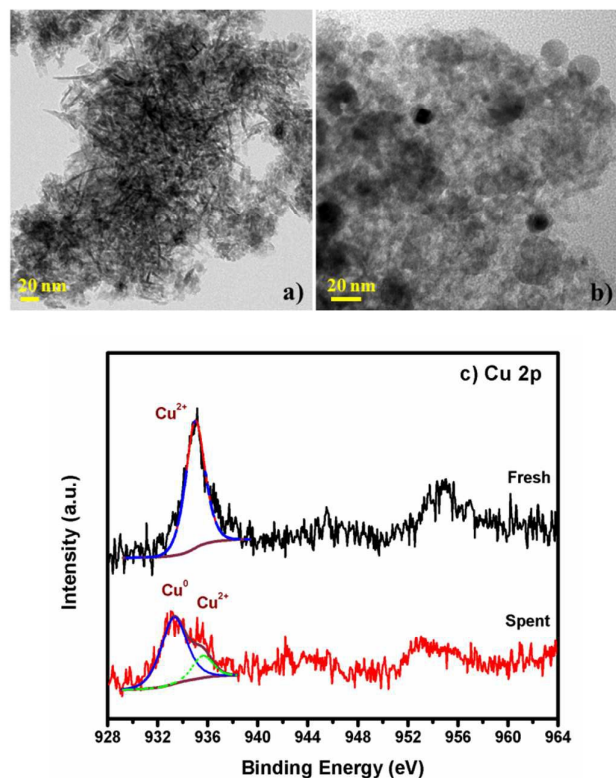
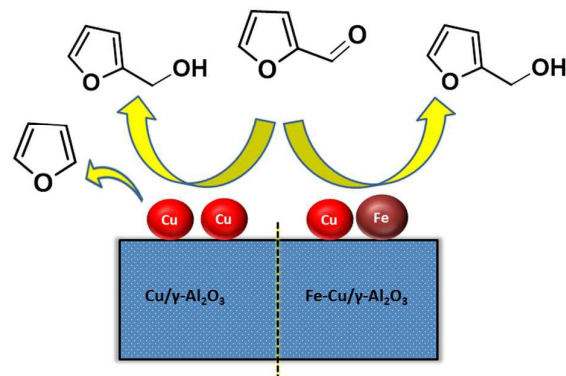


Fig. 10(a&b) are the TEM images of C-10 and FC-10 spent catalysts, respectively. c) XPS core level spectra of Cu for calcined and spent FC-10 catalyst.

It is also known that Cu has higher H₂ adsorption and activation abilities but a weaker oxygen affinity than Fe. According to the DFT calculations,⁴² it has been found that the metal–oxygen affinity of Fe is higher than FeCu bimetallic and Cu. For monometallic F-10 and C-10 catalysts, the oxygen vacancies on the iron oxide and Lewis acidic sites of alumina can bind oxygen atom of C=O group through the donation of the lone pair of electrons and subsequently the C=O bond is activated followed by hydrogenation.^{45,46} For bimetallic FC-X catalysts, carbonyl group oxygen is preferentially adsorbed on either Fe metallic or Fe oxides than metallic Cu sites and both Fe and Cu sites could be synergistically promoting the conversion of FAL. In other words, H₂ is easily dissociated on Cu sites and spills over to the neighboring Fe sites that is having adsorbed oxygen atom of a C=O group of FAL, where the hydrogenation takes place leading to the hydrogenation product. This phenomenon can be witnessed from Fig. 6b, i.e., the selectivity to FOL increased and decarbonylation suppressed with the Fe loading. This is obviously determinable to the promoting role of Fe for the selective hydrogenation as well as for reducing C-C hydrogenolysis. This promotional effect on the selective hydrogenation/hydrogenolysis owing to the increase in oxygen affinity of metal sites has also been reported over FeNi/SiO₂ catalysts.⁴²



Scheme 2. Schematic illustration of possible reaction pathway of FAL hydrogenation over monometallic Cu/ γ -Al₂O₃ and bimetallic Fe-Cu/ γ -Al₂O₃ catalysts.

Conclusions

Herein, we reported the synthesis of γ -Al₂O₃ supported FeCu based heterobimetallic system by simple co-impregnation method. The characterization results confirmed that the formation of FeCu bimetallic species during pre-treatment at 400 °C under H₂ flow. The conversion of FAL on FeCu/ γ -Al₂O₃ yields mainly FOL. The better catalytic activity with >98% FOL selectivity was achieved over a FC-10 catalyst under optimized reaction conditions. It was found that the addition of Fe enhances the activity that results in higher FAL conversion, whereas the selectivity was driven mostly by Cu. We discussed that the product distributions over various reaction parameters. The prolonged catalytic activity (up to 24 hours TOS) without any significant loss in activity was observed, proved the robustness of the catalyst. The analysis of spent catalysts also evidences that there was no morphology change and no significant increase in Cu particle size after the reaction. The plausible mechanism was proposed on the basis of products formed and the catalyst characterization results. The adsorption behavior of both Fe and Cu were also discussed. Further, the cooperative activity of FeCu system was extensively explained. Based on the studies we strongly believe that our presented work may induce to carving out Cr-free noble-metal-free innovative catalysts for the selective conversion of biomass derived compounds to fuels and chemicals.

Experimental section

Synthesis of catalysts

The FeCu/ γ -Al₂O₃ catalysts with different Fe loadings were prepared by incipient wetness impregnation method, using an aqueous solution containing both metal nitrate precursors Cu(NO₃)₂·6H₂O and Fe(NO₃)₃·9H₂O (98%, Merck). Boehmite derived γ -Al₂O₃ having a surface area of 182 m²/g was used as support, which was dried at 110 °C prior to impregnation. Then, aqueous solution containing the desired amount of metals was directly impregnated to the powdered γ -Al₂O₃ support. In all cases the content of Cu was kept constant

ARTICLE

Journal Name

at 10 wt% and Fe wt% was varied from 2.5 to 12.5 wt%. After impregnation, samples were first dried at room temperature for overnight and subsequently at 110 °C for 12 hours in oven. The obtained samples were calcined at 500 °C for 4 hours. For comparison, γ -Al₂O₃ supported Fe and Cu (10 wt%, respectively) were prepared with the procedures as same to those of FeCu/ γ -Al₂O₃ catalysts. Synthesized catalysts are labelled as FC-X, whereas X indicates the amount of Fe loading and FC stands for Fe and Cu, respectively. Where, F-10 and C-10 are the γ -Al₂O₃ supported monometallic catalysts containing 10 wt% of Fe and 10 wt% of Cu, respectively. The bulk compositions of catalysts were analyzed by ICP-OES, which were in good agreement with the theoretical values. All prepared catalysts were directly used after calcination.

Characterization techniques

Powder X-ray diffraction (XRD) data of synthesized materials were collected from PAN analytical X'pert Pro dual goniometer diffractometer. The chemical compositions of the synthesized catalysts were estimated by Inductively Coupled Plasma-Optical Emission Spectrometry (ICP-OES, Spectro Arcos, FHS-12). Temperature programmed reduction (TPR) and H₂-N₂O titration studies were carried out on Micrometrics 2920 instrument. Specific surface area, pore volume and average pore diameter of the materials were determined by nitrogen adsorption-desorption analysis at liquid nitrogen temperature (-196 °C) using AutosorbIQ Quantachrome, USA. The Brunauer-Emmett-Teller (BET) equation was used to calculate the surface area from the adsorption branch at a pressure range of (p/p₀ = 0.05 to 0.3). Pore volume and pore size measurements were calculated using Barret, Joyner and Halenda (BJH) method at a relative pressure of 0.99. A FEI TECNAI F20 electron microscope operating at 200 kV was used for recording high resolution transmission electron microscopy (TEM) of all materials. Iron and copper core levels were studied with X-ray photoelectron spectrometer (XPS) system from Prevac and equipped with VG Scienta monochromator (MX650) using AlK α anode (1486.6 eV).

Typical experiment and product analysis

The reactivity of catalysts for the vapour phase hydrogenation of FAL was evaluated in a vertical down flow stainless-steel fixed-bed reactor (8 mm inner diameter) at atmospheric pressure. In a typical run, 0.65 g (1 mL) of pelletized (size: 0.5–0.8 mm) catalyst was placed at the center of the Inconel alloy reactor by using ceramic beads and glass wool. The catalyst was pre-reduced in situ by H₂ flow (2400 gas hourly space velocity, GHSV h⁻¹) which is controlled by Brooks mass flow controller (5850 S) with a temperature increased from room temperature to 400 °C at a rate of 2 °C min⁻¹ and maintaining at 400 °C for 2 hours. After reduction, the reactor was cooled down to the desired reaction temperature (175–250 °C) under the same H₂ flow. A suitable flow of distilled FAL (Sigma-Aldrich, 99.5%, 0.6–2.4 mL hr⁻¹) was fed continuously from the high precision isocratic syringe pump and vapourized into the reactor. Then, H₂ flow was changed to 1200 GHSV h⁻¹.

The products were condensed using chiller and collected by every hour and the same were analyzed by Gas Chromatography (Varian-CP3800) with FID having HP-5 capillary column (30 m × 0.32 mm × 0.25 μ m). The carbon balances were checked in every run and found to be ranged between 98 and 101% and all data points were obtained in duplicate with an error of \pm 2%. The FAL conversion, FOL selectivity and yield were calculated and defined as follows:

$$\begin{aligned} \text{FAL conversion} &= \frac{\text{FAL}_{\text{in}} - \text{FAL}_{\text{out}}}{\text{FAL}_{\text{in}}} \\ \text{FOL selectivity} &= \frac{\text{FOL}_{\text{out}}}{\text{FAL}_{\text{in}} - \text{FAL}_{\text{out}}} \\ \text{FOL yield} &= \frac{\text{FAL conversion} \times \text{FOL selectivity}}{100} \end{aligned}$$

Acknowledgements

TR thanks the Department of Science and Technology, India-SERB (no. SR/S1/PC-17/2011) and CSC 0125 12 FYP for funding and MM thanks DST for fellowship.

References

- 1 M. Stöcker, *Angew. Chem., Int. Ed.*, 2008, **47**, 9200–9211.
- 2 J. N. Chheda, G. W. Huber and J. A. Dumesic, *Angew. Chem., Int. Ed.*, 2007, **46**, 7164–7183.
- 3 H. Olcay, A. V. Subrahmanyam, R. Xing, J. Lajoie, J. A. Dumesic and G. W. Huber, *Energy Environ. Sci.*, 2013, **6**, 205–216.
- 4 C. Somerville, H. Youngs, C. Taylor, S. C. Davis and S. P. Long, *Science*, 2010, **329**(5993), 790–791.
- 5 (a) A. S. Nagpure, A. Venugopal, N. Lucas, M. Manikandan, R. Thirumalaiswamy and S. Chilukuri, *Catal. Sci. Technol.*, 2015, **5**, 1463–1472; (b) E. Taarning, C. M. Osmondsen, X. B. Yang, B. Voss, S. I. Andersen and C. H. Christensen, *Energy Environ. Sci.*, 2011, **4**(3), 793–804.
- 6 A. Corma, O. de la Torre, M. Renz and N. Villandier, *Angew. Chem., Int. Ed.*, 2011, **50**, 2375–2378.
- 7 (a) J. P. Lange, E. van der Heide, J. van Buijtenen and R. Price, *ChemSusChem*, 2012, **5**, 150–166; (b) C. M. Cai, T. Zhang, R. Kumara and C. E. Wyman, *J Chem Technol Biotechnol* 2014, **89**, 2–10; (c) K. Yan, G. Wu, T. Lafleur, C. Jarvis, *Renew. Sust. Energ. Rev.*, 2014, **38**, 663–676
- 8 X. Li, J. Deng, J. Shi, T. Pan, C. G. Yu, H. J. Xu, and Y. Fu, *Green. Chem.*, 2015, **17**, 1038–1046.
- 9 (a) P. D. Carà, R. Ciriminna, N. R. Shiju, G. Rothenberg and Dr. M. Pagliaro, *ChemSusChem.*, 2014, **7**, 835–840; (b) X. Chena, H. Li, H. Luo and M. Qiao, *Appl. Catal. A: Gen.*, 2002, **233**, 13–20.
- 10 (a) M. L. Schlossman, US Pat., 4 301 046, 1981. (b) K. Yan, A. Chen., *Energy.*, 2013, **58**, 357–363.
- 11 H. Liu, Q. Hu, G. Fan, L. Yang and F. Li, *Catal. Sci. Technol.*, 2015, **5**, 3960.
- 12 (a) B.M. Nagaraja, V. Siva Kumar, V. Shasikala, A.H. Padmasri, B. Sreedhar, B. David Raju, K.S. Rama Rao, *Catal. Commun.*, 2003, **4**, 287–293; (b) B.M. Nagaraja, A.H. Padmasri, P. Seetharamulu, K. Hari Prasad Reddy, B. David Raju, K.S. Rama Rao, *J. Mol. Catal. A: Chem.*, 2007, **278**, 29–37.

- 13 (a) K. Yan, J. Liao, X. Wua and X. Xie, *RSC Adv.*, 2013, **3**, 3853–3856; (b) Y. Nakagawa and K. Tomishige, *Catal. Commun.*, 2010, **12**, 154.
- 14 V. P. Vladimír, N. Musselwhite, K. An, S. Alayoglu and G. A. Somorjai, *Nano Lett.*, 2012, **12**, 5196–5201.
- 15 J. Kijeński, P. Winiarek, T. Paryjczak, A. Lewicki, and A. Mikołajska, *Appl. Catal. A: Gen.*, 2002, **233**, 171.
- 16 M. Tamura, K. Tokonami, Y. Nakagawa and K. Tomishige, *Chem. Commun.*, 2013, **49**, 7034.
- 17 A. B. Merlo, V. Vetere, J. F. Ruggera and M. L. Casella, *Catal. Commun.*, 2009, **10**, 1665–1669.
- 18 (a) K. Fulajtárova, T. Soták, M. Hronec, I. Vávra, E. Dobrock, M. Omastová, *Appl. Catal. A: Gen.*, 2015, **502**, 78–85; (b) B. Chen, F. Li, Z. Huang, G. Yuan, *Appl. Catal. A: Gen.*, 2015, **500**, 23–29.
- 19 Y. Nakagawa, K. Takada, M. Tamura and K. Tomishige, *ACS Catal.*, 2014, **4**, 2718–2726.
- 20 D. E. Resasco, *J. Phys. Chem. Lett.*, 2011, **2**, 2294–2295.
- 21 S. K. Singh, A. K. Singh, K. Aranishi, and Q. Xu, *J. Am. Chem. Soc.*, 2011, **133**, 19638–19641.
- 22 (a) E. S. Gnanakumar, J. M. Naik, M. Manikandan, T. Raja and C. S. Gopinath, *ChemCatChem*, 2014, **16**, 11 3116–3124; (b) W. Yu, M. D. Porosoff and J. G. Chen, *Chem. Rev.*, 2012, **112**, 5780–5817.
- 23 (a) C.S. Chen, W.H. Cheng and S. S. Lin, *Appl. Catal.*, A, 257 (2004) 97–106; (b) K. Xiao, Z. Bao, X. Qi, X. Wang, L. Zhong, M. Lin, K. Fang, Y. Sun, *Catal. Commun.*, 2013, **40**, 154–157.
- 24 S. Sitthisa, W. An and D. E. Resasco, *J. Catal.*, 2011, **284**, 90–101.
- 25 H. Ando, Q. Xu, M. Fujiwara, Y. Matsumura, M. Tanaka and Y. Souma, *Catal. Today*, 1998, **45**, 229–234.
- 26 (a) K. Yan and A. Chen, *Fuel*, 2014, **115**, 101–108; (b) Y. Zhou, S. Wang, M. Xiao, D. Han, Y. Lub and Y. Meng, *RSC Adv.*, 2012, **2**, 6831–6837.
- 27 K. Kandel, U. Chaudhary, N. C. Nelson and I. I. Slowing, *ACS Catal.*, 2015, **5**, 6719–6723.
- 28 K. Pansanga, N. Lohitharn, A. C. Y. Chien, E. L. J. Panpranot, P. Praserttham, J. G. Goodwin Jr. *Appl. Catal. A: Gen.*, 2007, **332**, 130–137.
- 29 J. Stephen, Gentry and P. T. Walsl, *J. Chem. Soc., Faraday Trans. I*, 1982, **78**, 1515–1523.
- 30 Luo, C. Dai, A. Zhang, J. Wang, M. Liu, C. Song and X. Guo, *Catal. Sci. Technol.*, 2015, **5**, 3159.
- 31 (a) Z. H. Chonco, A. Ferreira, L. Lodya, M. Claeys, and E. van Steen, *J. Catal.*, 2013, **307**, 283–294; (b) K. Kandel, U. Chaudhary, N. C. Nelson and I. I. Slowing, *ACS Catal.*, 2015, **5**, 6719–6723.
- 32 E. S. Gnanakumar, K. S. Thushara, D. S. Bhange, R. Mathew, T. G. Ajithkumar, P. R. Rajamohanam, S. Bhaduri and C. S. Gopinath, *Dalton. Trans.*, 2011, **40**, 10936–10944.
- 33 S. R. Yan, K. W. Jun, J. S. Hong, M. J. Choi, K. W. Lee, *Appl. Catal. A: Gen.*, 2000, **194**, 63–70.
- 34 W. Cheng, K. Tang, Y. Qi, J. Sheng and Z. Liu, *J. Mater. Chem.*, 2012, **20**, 1799–1805.
- 35 I. Najdovski, P. R. Selvakannan, S. K. Bhargava and A. P. O'Mullane, *Nanoscale*, 2012, **4**, 6298–6306.
- 36 Y. Ye, L. Wang, S. Zhang, Y. Zhu, J. Shan and F. Tao, *Chem. Commun.*, 2013, **49**, 4385.
- 37 A. F. H. Wielers, C. E. C. A. Hop, J. V. Beijnum, A. M. Vander Kraan, and J. W. Geus, *J. Catal.*, 1990, **121**, 364–374.
- 38 C. C. Chusuei, M. A. Brookshier, and D. W. Goodman, *Langmuir*, 1999, **15**, 2806–2808.
- 39 Md. M. Rahman, S. B. Khan, H. M. Marwani, A. M. Asiri and K. A. Alamry, *Chemistry Central Journal*, 2012, **6**, 158.
- 40 K. Shimizu, H. Maeshima, H. Yoshida, A. Satsuma and T. Hattori, *Phys. Chem. Chem. Phys.*, 2000, **2**, 2435–2439.
- 41 S. Sitthisa and D. E. Resasco, *Catal. Lett.*, 2011, **141**, 784–791.
- 42 (a) S. Sitthisa, T. Pham, T. Prasomsri, T. Sooknoi, R. G. Mallinson, D. E. Resasco, *J. Catal.*, 2011, **280**, 17–27. (b) S. Sitthisa, W. An, D. E. Resasco, *J. Catal.*, 2011, **284**, 90–101.
- 43 R. V. Sharma, U. Das, R. Sammynaiken, A. K. Dalai, *Appl. Catal. A: Gen.*, 2013, **454**, 127–136.
- 44 S. Sitthisa, T. Sooknoi, Y. Mac, P. B. Balbuena, D. E. Resasco, *J. Catal.*, 2011, **277**, 1–13.
- 45 F. Delbecq and P. Sautet, *J. Catal.*, 1995, **152**, 217–236.
- 46 D. Loffreda, F. Delbecq, F. Vigne, P. Sautet, *Angew. Chem. Int. Ed.*, 2005, **44**, 5279–5282.